Report to DOE-BES

Abstract

Title: Nanoscale Molecules under Thermodynamic Control: Digestive Ripening or "Nanomachining"

Grant Number: DE-SC0005159

P.I. Names: Kenneth J. Klabunde (Chemistry, P.I.)
Christopher M. Sorensen (Physics, Co-P.I.)

Post doc : Deepa Jose

M.S. Student : Yijun Sun

Ph.D. Student: Jessica Changstrom

Affiliation: Kansas State University

Contact Information: Department of Chemistry
CBC 213
Manhattan, KS 66506
785-532-6849
kenjk@ksu.edu

Yearly Budget: $150,000

Period of Execution: Sept. 15, 2010 to Sept. 14, 2013

Overall Research Goals and Specific Objectives: Nanoscale materials are becoming ubiquitous in science and engineering, and are found widely in nature. However, their formation

processes and uniquely high chemical reactivities are not understood well, indeed are often mysterious.

Over recent years, a number of research teams have described nanoparticle synthesis, and aging, thermal treatment, or etching times have been mentioned. We have used the terms “digestive ripening” and “nanomachining” and have suggested that thermodynamics plays an important part in the size adjustment to monodisperse arrays being formed. Since there is scant theoretical understanding of digestive ripening, the overall goal in our research is to learn what experimental parameters (ligand used, temperature, solvent, time) are most important, how to control nanoparticle size and shape after initial crude nanoparticles have been synthesized, and gain better understanding of the chemical mechanism details.

Specific objectives for the past twentynine months since the grant began have been to

(1) Secure and train personnel;as of 2011, a postdoc Deepa Jose, female from the Indian Institute of Science in Bangalore, India; Yijun Sun, a second year graduate student, female from China; and Jessica Changstrom, female from the USA, GK12 fellow (program for enhancing teaching ability) are actively carrying out research.
(2) Find out what happens to sulfur bound hydrogen of thiol when it interacts with gold nanoparticles. Our findings are discussed in detail later.
(3) Determine the effect of particle size, shape, and temperature on dodecyl thiol assited digestive ripening of gold nanoparticles. See our discussions later.
(4) To understand in detail the ligand interaction in molecular clusters and nanoparticles
(5) Determine the effect of chain length of amines on Au nanoparticle size under digestive ripening conditions (carbon chain length varied from 4-18).
(6) Determine the catalytic activity of gold superlattices obtained by digestive ripening for oxidation of CO to CO_2 at room temperature.
(7) Determine the photocatalytic activity of metal nanoparticles like Au, Ag,Cu, and Pd supported on TiO_2 toward photocatalytic hydrogen production.

Significant Achievements and Results: We tried to understand why there is formation of molecular Au clusters like Au25 in some laboratories and why Au nanoparticles of 3500-5000

atoms (4-5 nm) are formed using our SMAD method in combination with digestive ripening. It has been clearly demonstrated in our recent paper in the Journal of Physical Chemistry Letters that during the formation of Au molecular clusters, Au being reduced by the thiols, whereas during the formation Au nanoparticles, surface cluster Au atoms are oxidized by thiols. Further to our research in the area of digestive ripening of Au nanoparticles, we found there is a size limit for digestive ripening to occur; millimeter and micron sized Au particles are not susceptible to digestive ripening by thiol, even at high temperatures. We confirmed the presence of a thiolate instead of a thiol when Au nanoparticles interact with thiol by quantifying the amount of hydrogen evolved during this process. This work is published in the Journal of American Chemical Society. A variety of amines with chain length varying from C4 to C18 were also used as ligands in the preparation of Au nanoparticles by the SMAD method and the inverse micelle method. The effect chain length of amines toward the particle size distribution of Au nanoparticles during the digestive ripening process was studied systematically and found that C12 amine (dodecylamine) is the best for the formation of monodisperse Au particles. It was also found that thiols are better capping ligands than amines for the preparation of Au nanoparticles. In addition to the size control study of Au nanoparticles during digestive ripening, we demonstrated the effectiveness of digestive ripening toward the formation of monodisperse Indium (In) and Indium sulfide (In_2S_3) nanoparticles. CdSe and CdTe quantum dots were also prepared by our SMAD method in combination with digestive ripening.

We also explored the catalytic activity of metal nanoparticles like Au, Pd, Ag, and Cu by loading them on TiO_2 matrix. A systematic study of photocatalytic hydrogen production using Au nanoparticles loaded onto a variety of TiO_2 nanoparticles (anatase, rutile, and P25) showed that Au nanoparticles acts as a sink for the photoexcited electrons and causes better charge separation. We did not observe any Au surface plasmon induced visible light activity to TiO2 semiconductor nanoparticles. Among the different metals used, Pd nanoparticles (0.25 wt %) loading showed the best photocatalytic hydrogen production, 2.5 mmols/h. One of the manuscripts of this work is under review and the other one is soon to be submitted.

Potential Impact: Control of digestive ripening has considerable significance for two important fields:

(1) Mineral Recovery: Gold mining, silver mining and other materials recovery could be affected;

(2) Catalysis: Controlling metal and metal oxide nanoparticle size and shape is crucial in developing selective catalysts for a wide variety of industrial processes.

(3) Water splitting and production of clean hydrogen gas has a considerable attention as a next generation energy carrier.

Description of Results

(1) Au Molecular clusters Vs Au nanoparticles: Size focusing

A complete study on size focusing of Au nanoparticles during ligand interactions was done. The most familiar and studied system is that of gold (metal) and thiol (ligand). Au molecular clusters were prepared by the Royce Murray's method and 4-5 nm sized Au nanoparticles were prepared by the solvated metal atom dispersion method or inverse micelle method in combination with digestive ripening. The methods of synthesis of these gold clusters vs gold nanoparticles are carefully compared. In the cluster case, an important intermediate is $(Au^{+}\ ^{-}SR)_n$ polymer, which is not the case in the synthesis of nanoparticles either from metal (vapor) atoms or metal ions. Also, it is shown that thiol can act as both a reductant ($Au^{3+} \longrightarrow Au^{1+}$), and as an oxidant ($Au^{0} \longrightarrow Au^{1+}$).

Thermodynamic forces are responsible for the favored formation of certain size clusters. Thiols react with Au(III) to produce Au(I)-SR polymer. Treatment of this thiol polymer with $NaBH_4$ causes reduction of some Au(I) to Au(0), but Au(I)-SR serves to cap and protect particularly stable very small gold cores. In this reaction scheme, Au(III) is reduced by thiol to form the Au(I)-SR thiolate polymer. On the other hand, both the SMAD method and Inverse Micelle method leads to Au atoms that rapidly aggregate to form Au(0) nanoparticles. Thiol reacts with these zero-valent particles to form surface Au(I)-SR capping structures. In this reaction scheme, Au(0) is oxidized by thiol, but only surface gold atoms are attacked.

Gold particle size has an influence on extent of reactivity with thiols. Certain thiols are more reactive in this way, and phenylethanethiol (PET) is more reactive than dodecanethiol (DDT) (at low temperature both DDT and PET reaction with surface gold atoms to quickly evolve H_2, however, PET reacts with butanone stabilized gold particles to form $Au^{+}SR^{-}$ polymer, but DDT does not).

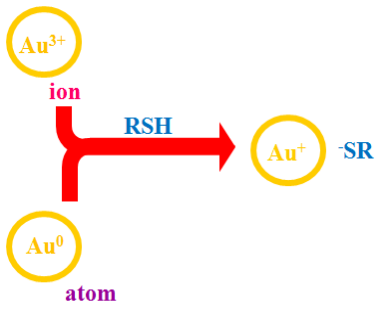

Figure 1: Thiol reduces gold(III) ion to gold(I) during the formation of molecular clusters and oxidizes gold atoms to gold(I) during the formation of nanoparticles (4-5 nm)

(2) Effect of Particle Size, Shape, and Temperature on Dodecylthiol Assisted Digestive Ripening of Gold Nanoparticles

Digestive ripening does occur readily with smaller sizes of 2-20 nm, and even with 40 or 50 nm Au nanoparticles in the presence of excess dodecylthiol and convert into thermodynamically preferred sizes of 4-6 nm. However, this “digestive ripening” process does not occur with large gold particles (micron or millimeter sizes). The presence of polar solvents, such as acetone, discourages digestive ripening in refluxing toluene (110 °C) or *tert*-butyltoluene (190 °C). Gold particles that are not brought up into solution through this digestive ripening process (precipitate left behind) grow even larger and more rounded in appearance, suggesting that even these larger particles do undergo changes induced by thiol attack, material transfer, and reprecipitation.

It is proposed that higher surface energies of smaller particles are partially responsible for these behaviors. Very small particles (below 4 nm) are vigorously attacked by thiol, and eventually torn apart and redeposited to form larger (4-6 nm) particles. Preferred particle size between 4-6 nm is most likely due to thiol/thiolate surface coverage and preferred curvature, which discourages further size reduction.

Scheme 1. Stepwise process of preparing solvated gold particles by the Solvated Metal Atom Dispersion (SMAD) method and then treatment under digestive ripening conditions

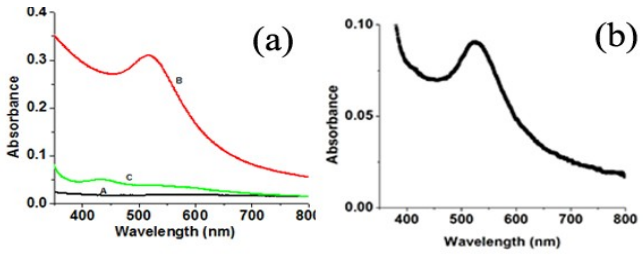

Figure 2. UV-visible absorption spectra for supernatant liquid in toluene: (a) A: before digestive Ripening in toluene; B: after 21 hours of digestive ripening in refluxing toluene (110 °C) under Ar with 30 equivalents RSH/Au; C: after repeating with additional RSH; (b) after pouring off the purple supernatant, addition of more RSH and toluene to the remaining gold precipitate, and 23 hours digestive ripening in *tert*-butyltoluene (190 °C).

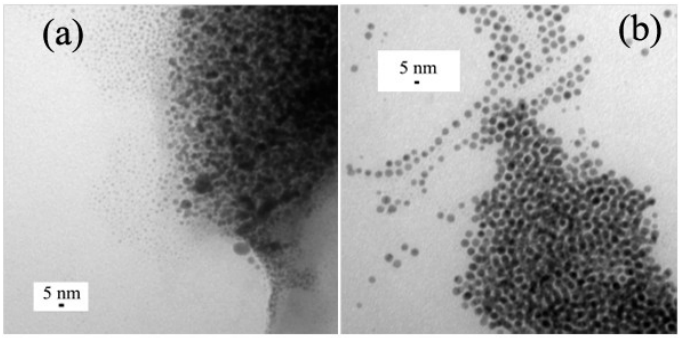

Figure 3**.** (a) TEM bright field images of gold nanoparticles prepared in THF after removal of THF (b) after addition of toluene and RSH to sample a and after digestive ripening in toluene (110 °C) for 24 hours.

Some general conclusions from these studies are as follows.

(1) There exist thermodynamically favored sizes, and for the gold/dodecylthiol system, 4.5-6 nm is the favored size range.

(2) Particles that are not brought up in solution do change tending toward more rounded, larger entities, showing that most, or all, of the gold is affected by the process.

(3) More coordinating SMAD solvents, especially acetone, tend to discourage the digestive ripening by thiol. It seems likely that acetone molecules remain bound to the gold surface and thus block attack by thiol.

(4) The least coordinating SMAD solvents, especially pentane and toluene, lead to the "cleanest" (least remaining SMAD solvent surface molecules) surface small particle gold, and are most susceptible to this digestive ripening process.

(5) The ripening process requires small particles, below about 20 nm, in order for these to be broken down to smaller, monodisperse systems in the range of 4-6 nm, depending on conditions. Larger particles of about 40-50 nm sometimes do undergo the process, but only if they are polycrystalline and under strain.[24]

(6) Smaller particles of 2-4 nm are readily consumed, and this part of digestive ripening is similar to Ostwald ripening.

(7) It seems reasonable to assume that smaller particles have higher surface energies, and this is responsible for thiol being able to attack. However, size preference in the 4-6 nm range must be related to thiol/thiolate coverage, that then discourages and eventually stops further size change.

(3) Loss of Hydrogen Upon Exposure of Thiol to Gold Clusters at Low Temperature

Gold-acetone-dodecanethiol and gold-acetone-phenylethanethiol colloids were prepared by the solvated metal atom dispersion (SMAD) method. Hydrogen evolution occurred at fairly low temperature, when the melting acetone-gold solvate encountered the thiol molecules, due to S-H bond scission. The gas inside the reactor was analyzed by gas chromatography, and the moles of H_2 determined by calibration curves obtained from a series of known concentration samples. The gold to thiolate ratio was calculated using thermal gravimetric analysis (TGA). The average particle diameter was also calculated using the gold to thiolate ratio.

These experiments show that the surface atoms of weakly solvated gold nanoparticles in the 2-8 nm size range are oxidized by thiols to yield hydrogen gas and thiolate stabilized nanostructures. Alternatively, the sulfur-hydrogen bond could be broken in a homolytic fashion, to form a RS-Au bond and hydrogen atoms, to yield hydrogen gas. An empirical formula of approximately Au_8SR was observed. For a 4 nm gold particle a molecular formula of about $Au_{2000}(SR)_{235}$ would be indicated. It should be noted that the hydrogen evolution occurs when thiol contacts the gold particles upon matrix meltdown and slow warmup to room temperature.

(4) Amine capped Au nanoparticles: Effect of chain length of amines toward particle size distribution during the digestive ripening process

Amine capped Au colloids were prepared by the SMAD method and by the inverse micelle method. Both alkyl and aryl amines were used with carbon chain length varying from 4 to 18.

For the gold alkyl-amine colloids synthesized by the inverse micelle method, the digestive ripening process greatly changed the particle size distribution, and transformed the polydispersed colloid into a monodispersed colloid. Short chain alkyl amines like Au-C4N and Au-C8N formed bigger particles which aggregate and settled down at the bottom whereas the long chain alkyl amines like Au-C12N, Au-C16N and Au-C18N gave 2D monolayers of small particles. Among the different alkyl amines used, dodecylamine gave the smallest particle sizes (8.8 ± 1.1 nm) with narrow size distribution.

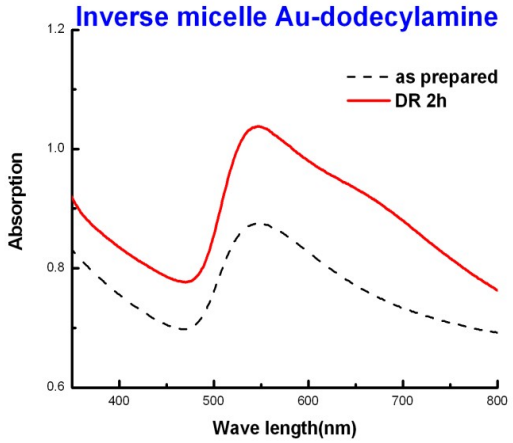

Figure 4. UV-Visible spectrum of Au-dodecylamine colloid by inverse micelle method before and after digestive ripening 2 h in toluene

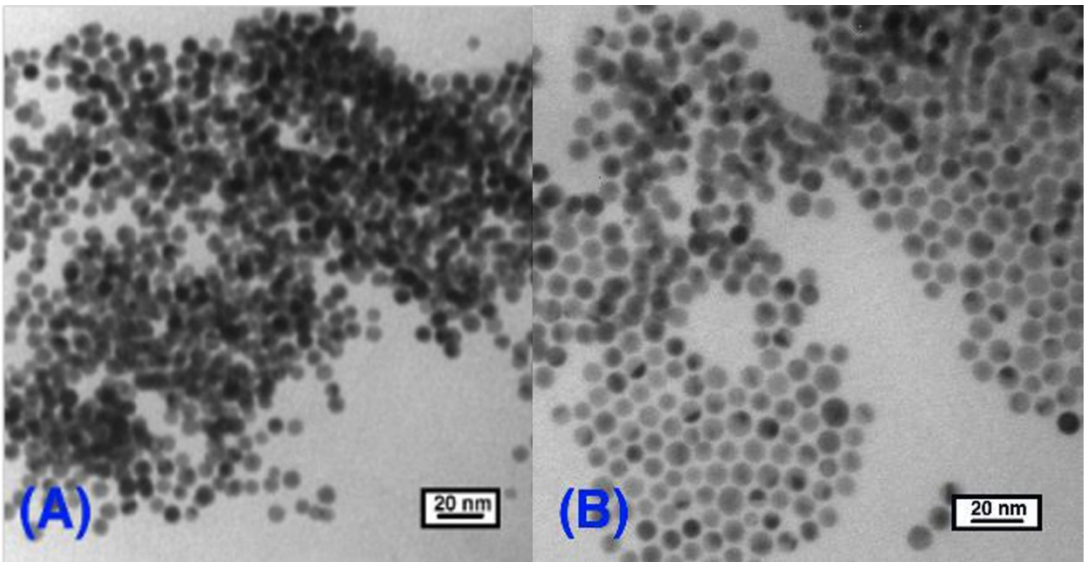

Figure 5. TEM images of (A) as prepared Au-dodecylamine colloid by inverse micelle method in toluene, (B) Au-dodecylamine colloid after digestive ripening 2h in toluene

(5) Synthesis of In nanoparticles and transformation of dodecanethiol capped In nanoparticles to Indium Sulfide upon digestive ripening

Monodispersed indium nanoparticles were synthesized by the solvated metal atom dispersion (SMAD) technique, followed by digestive ripening. Different surface active ligands (amine, phosphine, and mixed ligands) were used to passivate these indium nanoparticles. Digestive ripening was performed at two different temperature using a low boiling point solvent methylene chloride (BP 38°C) and a high boiling

point solvent toluene (BP 120°C). The as-prepared sample was polydisperse with particle size ranging from 25-50 nm, but upon digestive ripening in methylene chloride, a remarkable reduction of particle size was achieved. In higher boiling solvent (toluene), where the indium nanoparticles at reflux temperature are probably melted, it does not allow the best result, and less monodispersity is achieved. The temporal evolution of the surface plasmon of indium nanoparticles was monitored by in situ UV-Vis spectroscopy and particles were characterized by transmission electron microscopy (TEM) and X-ray diffraction (XRD). The merits of this synthesis procedure are the use of bulk Indium as starting material, tuning the particle size in low boiling point solvent, particle size adjustment with the choice of ligand and a possible scale up.

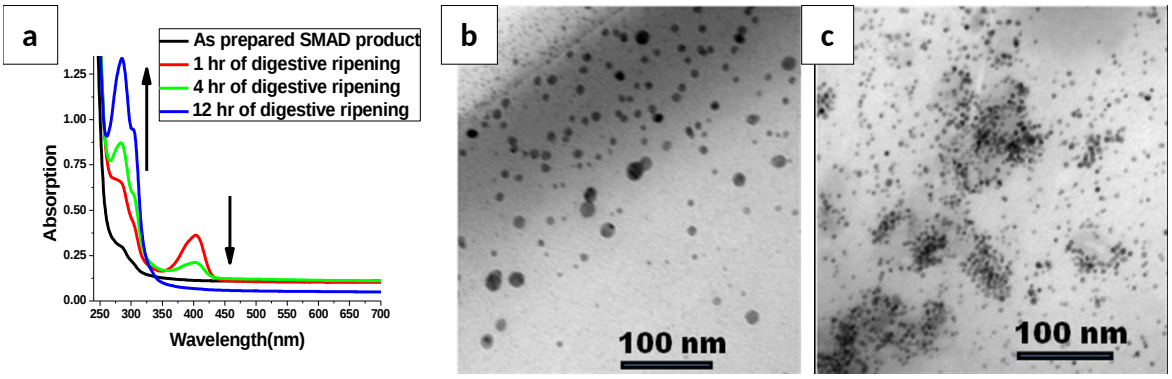

Figure6. (a) Temporal evolution of surface plasmon peak of indium nanoparticles with digestive ripening in low boiling point methylene chloride, (b) transmission electron microscopy image of before digestive ripening polydispersed indium nanoparticles and (c) monodispersed indium nanoparticles after digestive ripening.

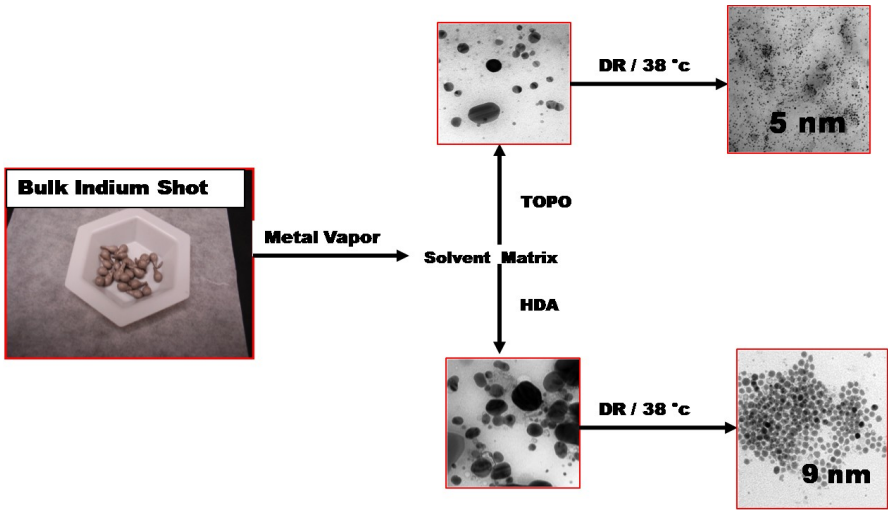

Figure7: Pictorial representation of indium nanoparticles synthesis.

Dodecanethiol also was used as a surfactant to stabilize In nanoparticles. However, these In nanoparticles were transformed into highly monodispersed β-indium sulfide upon digestive ripening in t-butyltoluene (190 °C). The transformed product (In_2S_3) was characterized with UV-Vis, XRD, EDX, SEM, XPS, and TEM. The visible light-induced photocatalytic activity test with In_2S_3 nanoparticles showed the 95 % of Rhodamine B and methyleneblue dye degradation after 100 min of visible light irradiation. The overall, transformation is shown in Figure 8.

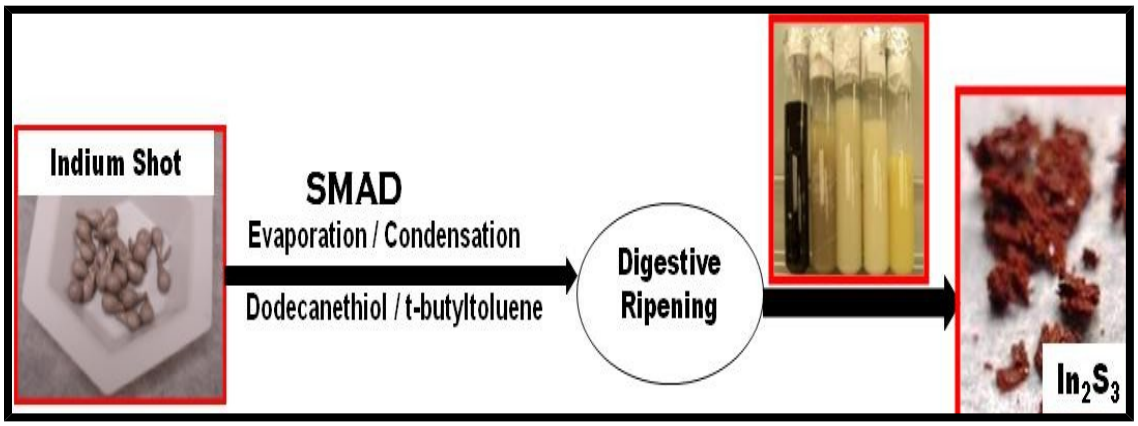

Figure8: Transformation of dodecanethiol indium nanoparticles to indium sulfide upon digestive ripening in t-butyl toluene solvent.

(6) Synthesis of CdSe and CdTe quantum dots and refined digestive ripening

CdSe and CdTe quantum dots (QDs) from the bulk CdSe and CdTe material were prepared by the solvated metal atom dispersion (SMAD) technique, followed by refined digestive ripening. In refined

digestive ripening, the ligands (Trioctylphosphine oxide and oleylamine) were used as capping agents as well as digestive ripening solvent. The outcomes of this new process are (1) the reduction of particle growth time period (digestive ripening time), (2) ability to tune the photoluminescence (PL) from 410 nm to 670 nm, (3) demonstration of the ability of SMAD synthesis technique for semiconductors, (4) direct comparison of CdSe QDs growth with CdTe QDs growth based on digestive ripening time , and (5) enhanced PL quantum yield (QY) of CdSe QDs and CdTe QDs upon application of a ZnS shell. The merit of this synthesis is the use of bulk CdSe and CdTe as the starting material, which avoids usage of toxic organometallic compounds, eliminates the hot injection procedure, eliminates the need for size selective precipitation process, and has the possibility of scale up. These QDs were characterized by UV-Vis, PL, transmission electron microscopy (TEM), high resolution transmission electron microscopy (HRTEM), XPS, and XRD. The new procedure was depicted in Figure 9.

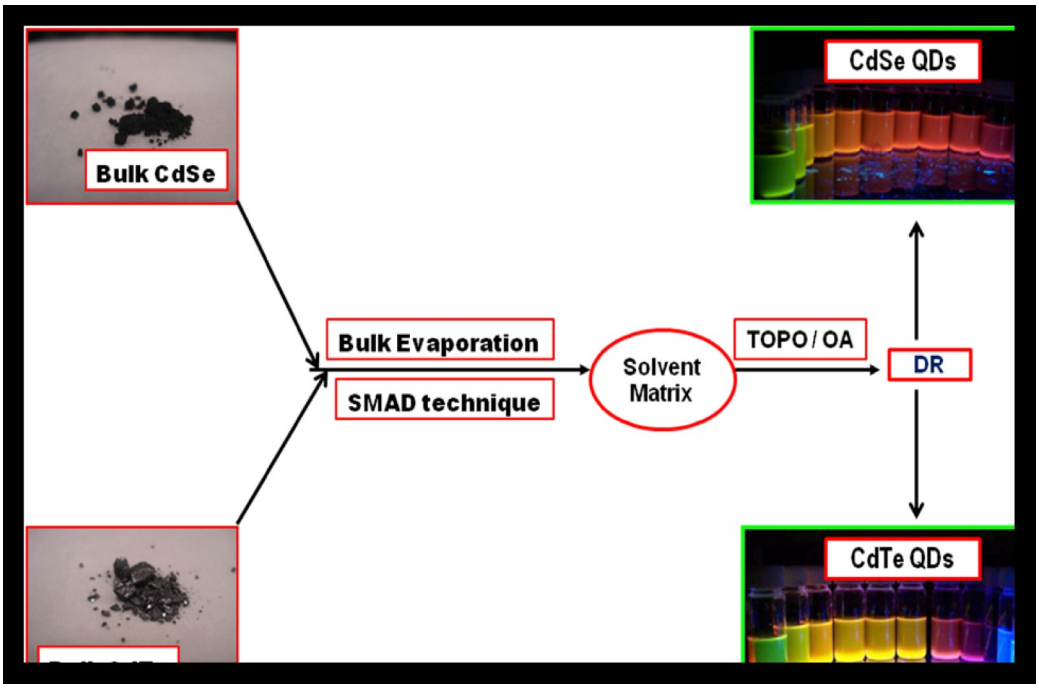

Figure 9. Schematic representation of synthesis of cadmium selenide and cadmium telluride QDs by the SMAD technique, followed by refined digestive ripening.

(4) Solvated Metal Dispersion method for the Gram Scale Synthesis of Au-TiO_2 Nanocomposites and Efficient Photocatalytic Hydrogen Production under UV-visible Light Illuminations

$Au_{(\sim 1\ wt\%)}/TiO_{2(anatase\ or\ rutile\ or\ P25)}$ nanocomposites were prepared by the solvated metal atom dispersion (SMAD) method and the as-prepared samples were characterized by diffuse reflectance UV-visible spectroscopy, powder XRD, BET surface analysis measurements, and transmission electron microscopy bright field imaging. The particle size of the embedded Au nanoparticles ranged from 1-10 nm. These Au/TiO_2 nanocomposites were used for photocatalytic hydrogen production in the presence of a sacrificial electron donor like ethanol or methanol under UV-visible and visible light illumination. These nanocomposites showed very good photocatalytic activity toward hydrogen production under UV-visible conditions whereas under visible light illumination there was not much enhancement. Au/P25 gave a hydrogen evolution rate of 1600 μmol/h in the presence of ethanol (5 volume %) under UV-visible illumination. In the case of Au/TiO_2 prepared by the SMAD method the presence of Au nanoparticles serves two purposes: as an electron sink gathering electrons from the conduction band (CB) of TiO_2, and as a reactive site for water/ethanol reduction to generate hydrogen gas. We also observed hydrogen production by water splitting in the absence of a sacrificial electron donor using Au/TiO_2 nanocomposites under UV-visible illumination.

Catalyst	**Rate (μmol/h)**		
	Dark	**visible**	**UV-visible**
No catalyst	0.0	0.0	2.2
P25	0.0	1.9	90
Au/P25	0.0	6.9	1600
Anatase commercial	0.0	0.0	1.7
Au/anatase commercial	0.0	0.0	300
Anatase aerogel	0.0	0.0	18
Au/anatase aerogel	0.0	0.0	1200
Rutile	0.0	3.3	6.3
Au/rutile	0.0	5.6	530

Table 1. Amount of Hydrogen evolved using Au/TiO_2 nanocomposites under dark, visible, and UV-visible photocatalytic runs for 5 h in the presence of ethanol (5 volume %) using a 450 W Mercury lamp

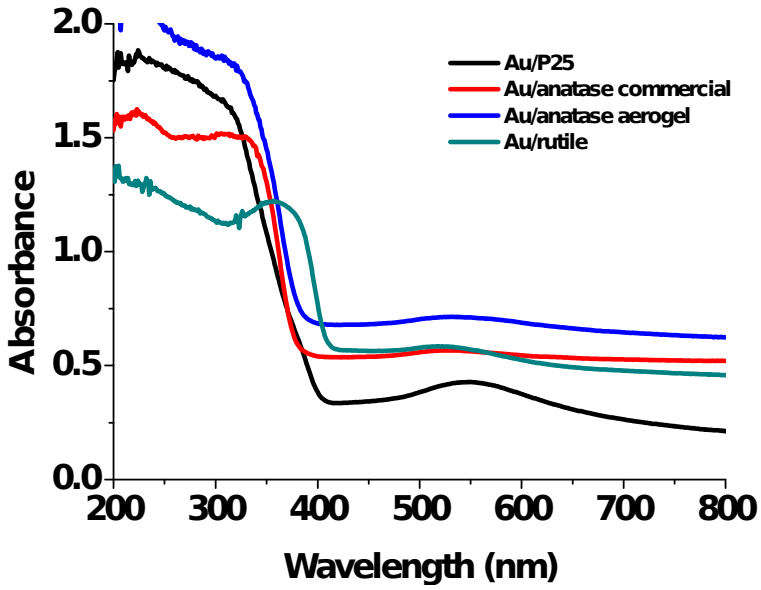

Figure 10. Diffuse reflectance UV-visible spectra of Au/TiO2 nanocomposites prepared by solvated metal atom dispersion method

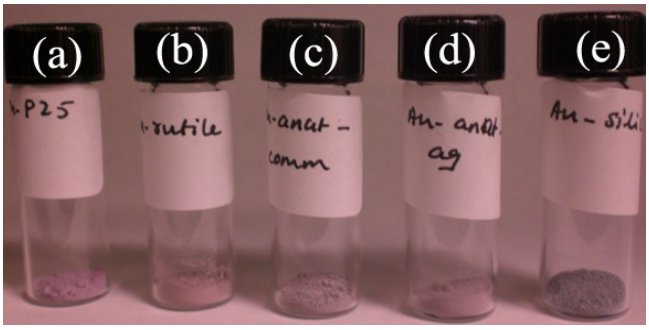

Figure 11. Photographs of different photocatalysts prepared by SMAD method: (a) Au/P25, (b) Au/rutile, (c) Au/anatase commercial, (d) Au/anatase aerogel, and (e) Au-silica

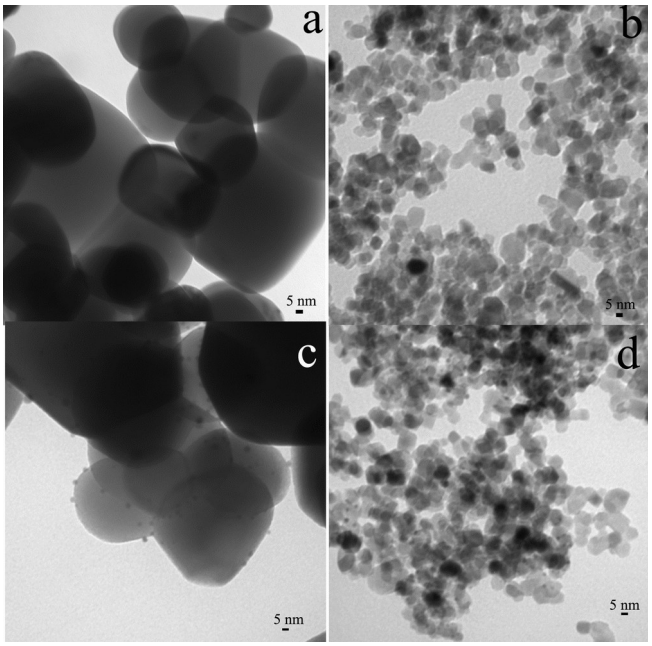

Figure 12. TEM bright field image of TiO2 and Au/TiO2 prepared by SMAD method: (a) anatase commercial, (b) anatase aerogel, (c) Au/anatase commercial, and (d) Au/anatase aerogel

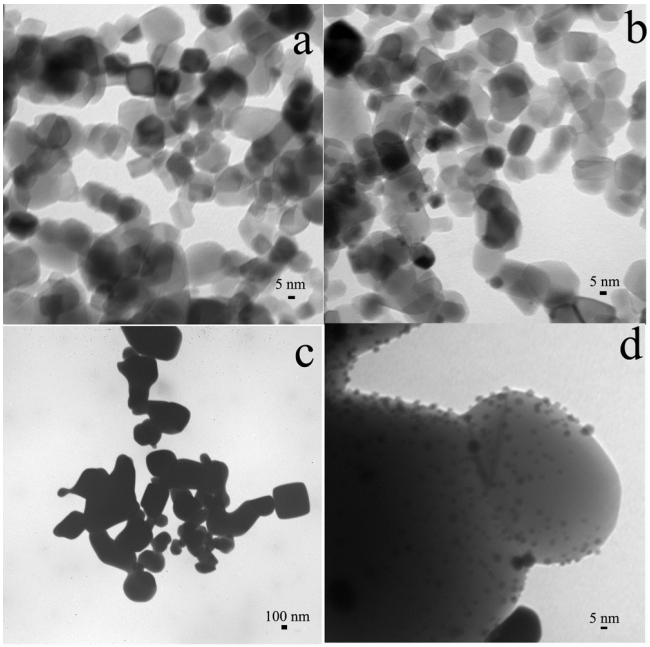

Figure 13. TEM bright field images of TiO_2 and Au/TiO_2 prepared by the SMAD method (a) P25, (b) Au/P25, (c) rutile, and (d) Au/rutile

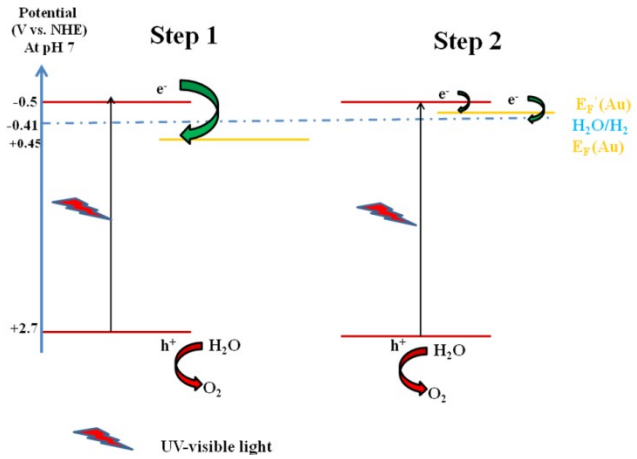

Figure 14. Elementary steps showing photocatalytic water splitting under UV-visible illumination using Au/TiO_2 nanocomposites: Step 1 is electron transfer from the CB of photoexcited TiO_2 to Au Fermi level and Step 2 is Au Fermi level shift to negative potential by gathering photoexcited electrons from TiO_2 and water reduction

(5) Enhanced Photocatalytic Hydrogen Production from TiO_2 Semiconductor Nanoparticles by Pd loading

Nanoparticles of metals like Au, Ag, Pd, and Cu were loaded on to P25 TiO_2 by the solvated metal atom dispersion (SMAD) method. These M/TiO_2 nanocomposites were characterized by the DRS UV-visible spectroscopy, transmission electron microscopy, powder XRD, and BET surface area analysis. Photocatalytic hydrogen evolution from ethanol/water mixture was tested under UV-visible conditions using these nanocomposites and Pd/TiO_2 sample (0.25 wt % Pd) showed the best photocatalytic activity with a hydrogen evolution rate of 2500 μmol/h (Table 2). The photocatalytic activity of Pd/TiO_2 samples was also tested in the presence of an inorganic sacrificial agent like sodium sulfite (50 mM) and in the absence of a sacrificial agent (Table 3). In the presence of sodium sulfite as a sacrificial electron donor pure hydrogen evolution takes place by pure water splitting. We observed hydrogen evolution even in the absence of a sacrificial agent, indicating that loaded Pd nanoparticles can act as a sink for photogenerated electrons and charge separation takes place. We expected both hydrogen and oxygen evolution by over all water splitting; but no oxygen evolution was observed which could be due to the high solubility of oxygen in water.

The effect of chain length and presence of a hydrogen atom alpha to the alcohol group toward photocatalytic hydrogen evolution were also studied (Table 4). It was found that presence of a hydrogen atom alpha to the alcohol group is essential for better photocatalytic hydrogen evolution from alcohols. CeO_2 and $SrTiO_3$ were also used for Pd loading and the effect of different semiconductors used for Pd loading and photocatalytic hydrogen production were studied. In our studies TiO_2 showed the best result compared to CeO_2 and $SrTiO_3$ (Table 5).

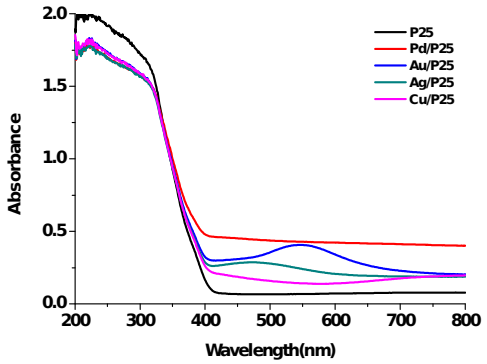

Figure 15. DRS-UV-visible spectra of 0.25 wt % Pd, Au, Ag, or Cu nanoparticles loaded onto TiO_2 nanoparticles by the SMAD method

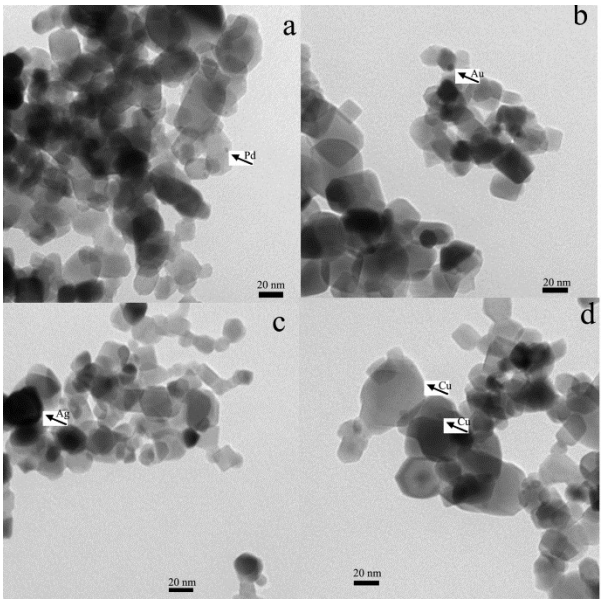

Figure 16. TEM bright field images of the SAMD prepared M/TiO_2 nanocomposites: (a) Pd/P25, (b) Au/P25, (c) Ag/P25, and (d) Cu/P25

M/P25 nanocomposite (0.25 wt % M)	Rate (5 vol % ethanol) in water
Pd/P25	2500 μmol/h
Au/P25	487 μmol/h
Cu/P25	373 μmol/h
Ag/P25	45 μmol/h

Table 2. Photocatalytic hydrogen production from M/P25 nanocomposites using a variety of metals under UV-visible illumination

Pd/P25 (Pd wt %)	Ethanol (5 vol %)	Sodium sulfite (50 mM)	No electron scavenger
0	90 μmol/h	9 μmol/h	0 μmol/h
0.25	2500 μmol/h	83 μmol/h	58 μmol/h
0.5	2500 μmol/h	71 μmol/h	44 μmol/h
1.0	1700 μmol/h	62 μmol/h	47 μmol/h
5.0	1500 μmol/h	49 μmol/h	47 μmol/h

Table 3. Effect Pd loading on Photocatalytic hydrogen production in Pd/P25 nanocomposites under UV-visible illumination in the presence and absence of a sacrificial electron donor

Sacrificial electron donor (5 vol %)	Rate
methanol	2300 μmol/h
ethanol	2.5 mmol/h
propanol	826 μmol/h
Iso-propanol	2.3 mmol/h
butanol	848 μmol/h
t-butyl alcohol	163 μmol/h
diglyme	326 μmol/h

Table 4. Photocatalytic hydrogen production from Pd/P25 nanocomposites under UV-visible illumination using a variety of alcohols

Photocatalyst used	Rate
P25	90 μmol/h
Pd/P25	2500 μmol/h
$SrTiO_3$	4 μmol/h
Pd/$SrTiO_3$	14 μmol/h
CeO_2	1 μmol/h
Pd/CeO_2	4 μmol/h

Table5. Photocatalytic hydrogen production using Pd nanoparticles (0.25 wt %) loaded on to a variety of semiconductors using 5 volume % ethanol under UV-visible illumination using a 450 W mercury lamp

Objectives for the Next Granting Period: At the end of this granting period, we have learned a great deal about manipulating metal particles. It is now possible to prepare on large scale monodisperse gold, silver, palladium, cobalt, cadmium selenide, and other important materials. It is now also possible to prepare on large scale nanocrystal superlattices that exhibit very interesting optical properties, absorbing visible radiation in the 600-700 nm range.

For about a year, we tried to use our expertise in metal nanoparticle preparation and manipulation to create new composites of gold and palladium particles with TiO_2 semiconductors for photocatalytic hydrogen production from water and water/ethanol solutions. We did succeed in producing large amounts of hydrogen. However, after many attempts, it was determined that this was only possible when hole scavengers (such as ethanol, methanol, other alcohols, or sulfites) were present. It was not possible to produce oxygen and hydrogen from water.

Therefore, it was decided that for the next granting period, we would bring in an expert on solar cell design, and try to use our nanocrystal superlattices as components of new solar cells that absorb light over a broad visible light spectrum.

Thus, Dr. Jun Li will be the P.I. on the next proposal. He will take the place of K.J. Klabunde, who will be retiring in August of 2013.

Statement of Unspent Funds for the Year: We estimate that by September 15, 2013, all of the grant fund will be spent.

List of Pending and Current Support:

K.J. Klabunde (Active)

- Nanotechnology for Renewable Energy, National Science Foundation-EPSCoR; $40,000/year; 10/01/2009-09/30/2014.
- Nanoscale Molecules under Thermodynamic Control: Digestive Ripening of Nanomachining; Department of Energy; $150,000/year; 09/15/2010-09/14/2013 (with C.M. Sorensen)

Christopher M. Sorensen (Pending)

- Kansas Center for Nanophotonics; National Science Foundation; $500,000/year; 08/01/2011-07/31/2016.
- Development of a Water Based, Critical Flow, Non-Vapor Compression Cooling Cycle; U.S. Dept. of Energy; $143,000/year; 09/1/2010-08/31/2013.

Complete List of Publications since 2011:

- Sole Funding by DOE-BES:

  Jose, D.; Matthiesen, J. E.; Parsons, C.; Sorensen, C. M.; Klabunde, K. J. "Size Focusing of Nanoparticles by Thermodynamic Control through Ligand Interactions. Molecular Clusters Compared with Nanoparticles of Metals", *J. Phys. Chem. Lett.* **2012,** *3***,** 885-890.

  Cingarapu, S.; Yang, Z.; Sorensen, C.M.; Klabunde, K.J.; "Synthesis of CdSe/ZnS and CdTe/ZnS Quantum Dots: Refined Digestive Ripening" *J. Nanomater.* **2012,** *312087*, 1-12.

- Joint Funding by DOE and other Funding Sources:

  Matthiesen, J. E.; Jose, D.; Sorensen, C. M.; Klabunde, K. J. "Loss of Loss of Hydrogen Upon Exposure of Thiol to Gold Clusters at Low Temperature", *J. Am. Chem. Soc.* **2012**, *134*, 9376−9379.

  Cingarapu, S.; Yang, Z.; Sorensen, C. M.; Klabunde, K. J.; "Synthesis of Indium Nanoparticles: Digestive Ripening under Mild Conditions," *Inorganic Chemistry* 2011, *50***,** 5000-5005.

  Cingarapu, S.; Hamal, D. B.; Ikenberry, M. A.; Sorensen, C. M.; Hohn, K.; Klabunde, K. J. "Transformation of Indium Nanoparticles to β-Indium Sulfide: Digestive Ripening and Visible Light Induced Photocatalytic Properties," *Langmuir* **2012,** *28*, 3569-3575.

- Sole Funding by Other Funding Sources:

  Kuo, Y., Klabunde, K. J. “Hydrogen from Ethanol Solution under UV-visible Light. Photocatalysts Produced by Nitriding Titanium Nitride and Indium Oxide Intimate Mixtures to Form Ti-In Nitride Composites,” *Applied Catalysis B: Environmental* **2011,** *104*, 245-251.

  Sub; W. H.; Sreeram, C.; Klabunde, K. J.; Law, B. M. “Nanoparticle Adsorption at Liquid-Vapor Surfaces: Influence of Nanoparticle Thermodynamics, Wettability, and Line Tension,” *Langmuir* **2011,** ***27***, 9979-9984.

  Hamal, D. B., Klabunde, K. J.; “Valence State and Catalytic Role of Cobalt Ions in Cobalt TiO_2 Nanoparticle Photocatalysts for Acetaldehyde Degradation under Visible Light,” *J. Phys. Chem. C* **2011,** *115*, 17359-17367.

  Mahendar, K.; Sarma, A.V.S.; Raghavaiah, P.; Kantam, M. L.; Klabunde, K. J. “Synthesis of β-Hydroxy α-Sulfanyl Esters by Using Nanocrystalline Magnesium Oxide,” *Helvetica Chimica Acta* **2011**, *94*, 1533-1542.

  Kantam, M.L.; Priyabarshini, S.; Srinivas, P.; AmalJoseph, P.J. Vinu, A.; Klabunde, K.J.; “Catalytic Guanylation of Aromatic and Secondary Amines using Nanocrystalline Zinc (II) Oxide,” *Tetrahedron* **2012,** *68*, 5730–5737.

  Kalita, M.; Cingarapu, S.; Santanu, P.; Park, S.; Higgins, D.; Jankowiak, R.; Chikan, V.; Klabunde, K.J.; Bossmann, S.; “Direct Synthesis of Aqueous Quantum Dots through 4,4’-Bipyridine-Based Twin Ligand Strategy,” *Inorganic Chemistry* **2012,** *51*, 4521-4526.

  Kuo, Y-T.; Klabunde, K. J. “Hydrogen Generation from Water/Methanol under Visible Light using Aerogel Prepared Strontium Titanate ($SrTiO_3$) Nanomaterials Doped with Ruthenium and Rhodium Metals,” *Nanotechnology* **2012,** *23*, 294001.

  Ilyina, E.V.; Mishakov, I.V.; Vedyagin, A. A.; Cherepanova, S.V.; Nadeev, A. N.; Bedilo, A. F.; Klabunde, K. J. “Synthesis and Characterization of Mesoporous VO_x/MgO Aerogels with High Surface Area.” *Microporous and Mesoporous Materials* **2012,** *160*, 32-40.

  Wi, Haeng Sub; Sreeram; C.; Klabunde, K. J.; Sorensen, C. M.; Law, B. M. “Observation of Nanoparticle-Enhanced Marangoni Transport Near a Freezing Out Front.” *J. Phys. Chem. C* **2012,** *116*, 6052-6057.

  Kuo, Y.T.; Frye, C.D.; Ikenberry, M.; Klabunde, K. J.; “Titanium-Indium Oxy(nitride) with and without RuO_2 Loading as Photocatalysts for Hydrogen Production under Visible Light from Water,” *Catalysis Today* **2013,** *199*, 15-21.

Peiris, Manindu Thelge; Klabunde, Kenneth J.; “Photocatalysts for Elimination of Toxins on Surfaces and in Air using UV and Visible Light,” invited book chapter in *Catalysis for Remediation and Environmental Concerns*, *First Edition*; editor Steven L. Suib, Elsevier Publishers, Amsterdam (2012).

Klabunde, K.J.; Koper, O.; Khaleel, A.; “Porous Pellet Adsorbents Fabricated from Nanocrystals.” Japanese Patent Number **4959051**, March 30, 2012.

Koper, Olga; Kwen Haidoo; Toerber, Scott; Knappenberger, Kyle; Jones, David; Basco, Debbie; Klabunde, Kenneth; Sanford, Bill; “treatment of Odors Using Nanocrystalline Metal Oxides,: U.S. Patent **8,038,935**, October 8 (2011).

LIST OF PUBLICATIONS THAT ACKNOWLEDGED DOE-BES CATALYSIS GRANTS/PWPs

	A	B	C	D	E	F	G	H	I	J	K	L	M	N	O
1	**Grant/FWP**	**Grant/FWP**	**Grant/FWP**	**Other**	**Publication Title**	**journal**	**volume**	**Page range**	**Year**	**Author 1**	**Author 2**	**Author 3**	**Author 4**	**Author 5**	**Author 6**
2	**Number**	**Institution**	**PI**	**funding**		**Book Title**									
3						**or Patent Reference**									
4															
5	DE-SC0005160	KSU	Klabunde K J		Size focusing of Nanopareticles	Journal	3	885-890	2012	Jose, D.	Matthiesen, J. E.	Parsons, C.	Sorensen, C.M.	*Klabunde, K.J.	
6					by Thermodynamic Control through	of Physical hemistry									
7					Ligand Interactions. Molecular	Letters									
8					Clusters Compared with										
9					Nanoparticles of Metals										
10															
11	DE-FG 02--10	KSU	Klabunde K J		Synthesis of CdSe/ZnS and CdTe/ZnS	Journal of	2012	01-0012	2012	Cingarapu, S.	Yang, Z.	Sorensen, C.M.	*Klabunde, K.J.		
12	ER16202				Quantum Dots:Refined digestive	Nanomaterials									
13					Ripening										
14															
15	DE-SC0005160	KSU	Klabunde K J	REU	Loss of Hydrogen Upon Exposure of	Journal of									
16					thiol to Gold Clusters at Low	American Chemical	134	9376–9379	2012	Matthiesen, J. E.	Jose, D.	Sorensen, C.M.	*Klabunde, K.J.		
17					Temperatures	Society									
18															
19	DOE (DESC000	KSU	Klabunde K J	NSF (CT 5060	Transformation of Indium										
20	5159)			9318)	Nanoparticles to β-Indum Sulfide:	Langmuir	28	3569-3575	2012	Cingarapu, S.	Ikenberry, M.	Hamal, D. B.	Sorensen, C.M.	Hohn, K.	*Klabunde, K.J.
21					Digestive Ripening and Visible										
22					Light Induced Photocatalytic										
23					Properties										
24															
25	DE-SC0005160	KSU	Klabunde K J	NSF (CT 5060	Synthesis of Indium Nanoparticles										
26				9318)	Digestive Ripening under	Inorganic Chemistry	50	5000-5005	2011	Cingarapu, S.	Yang, Z.	Sorensen, C.M.	*Klabunde, K.J.		
27					Mild Conditions										
28															